# Sequence Context- and Temperature-Dependent Nucleotide Excision Repair of a Benzo[*a*]pyrene Diol Epoxide-Guanine DNA Adduct Catalyzed by Thermophilic U*vr*ABC Proteins†

Qian Ruan,‡ Tongming Liu,‡ Alexander Kolbanovskiy,‡ Yang Liu,‡ Jian Ren,‡ Milan Skorvaga,§,|| Yue Zou,⊥ Joshua Lader,‡ Brijesh Malkani,‡ Shantu Amin,# Bennett Van Houten,§ and Nicholas E. Geacintov*,‡

*Chemistry Department, New York University, 31 Washington Place, New York, New York 10003-5180, Laboratory of Molecular Genetics, NIEHS, National Institutes of Health, Research Triangle Park, North Carolina 27709, Department of Molecular Genetics, Cancer Research Institute, Slovak Academy of Sciences, Vlarska 7, 833 91 Bratislava, Slovakia, Department of Biochemistry and Molecular Biology, James H. Quillen College of Medicine, East Tennessee State University, Johnson City, Tennessee 37614, and Department of Pharmacology, Penn State College of Medicine, Hershey, Pennsylvania 17033*

*Received February 10, 2007*

ABSTRACT: The influence of DNA base sequence context on the removal of a bulky benzo[*a*]pyrene diol epoxide-guanine adduct, (+)-*trans*-B[*a*]P-$N^2$-dG (G*), by UvrABC nuclease from the thermophilic organism *Bacillus caldotenax* was investigated. The lesion was flanked by either T or C in otherwise identical complementary 43-mer duplexes (TG*T or CG*C, respectively). It was reported earlier that in the CG*C context, a dominant minor groove adduct structure was observed by NMR methods with all Watson−Crick base pairs intact, and the duplex exhibited a rigid bend. In contrast, in the TG*T context, a highly flexible bend was observed, base pairing at G*, and two 5′-base pairs flanking the adduct were impaired, and multiple solvent-accessible adduct conformations were observed. The TG*T-43-mer duplexes are incised with consistently greater efficiency by UvrABC proteins from *B. caldotenax* by a factor of 2.3 ± 0.3. The rates of incisions increase with increasing temperature and are characterized by linear Arrhenius plots with activation energies of 27.0 ± 1.5 and 23.4 ± 1.0 kcal/mol for CG*C and TG*T duplexes, respectively. These values reflect the thermophilic characteristics of the UVrABC nuclease complex and the contributions of the different DNA substrates to the overall activation energies. These effects are consistent with base sequence context-dependent differences in structural disorder engendered by a loss of local base stacking interactions and Watson−Crick base pairing in the immediate vicinity of the lesions in the TG*T duplexes. The local weakening of base pairing interactions constitutes a recognition element of the UvrABC nucleotide excision repair apparatus.

Among the different DNA repair pathways, nucleotide excision repair (NER) constitutes a mechanism that recognizes bulky DNA lesions (*1*, *2*). DNA adducts derived from environmental polycyclic aromatic hydrocarbon (PAH) carcinogens are examples of bulky DNA adducts that are repaired by prokaryotic (*3*−*6*) and eukaryotic (*7*) NER pathways. Benzo[*a*]pyrene (B[*a*]P), a widely studied PAH compound (*8*), is metabolized to the highly mutagenic and tumorigenic diol epoxide enantiomer (+)-7*R*,8*S*-dihydroxy-9*S*,10*R*-epoxy-7,8,9,10-tetrahydrobenzo-[*a*]pyrene ((+)-*anti*-B[*a*]PDE). The latter binds predominantly to the exocyclic amino group of guanine in native DNA (*9*).

Much of what is known about the removal of bulky adducts by prokaryotic NER comes from extensive studies of the repair pathways in *Escherichia coli* (*10*, *11*). The general mechanism involves the interaction of two UvrA molecules that form $UvrA_2$ dimers in solution (*12*). The dimers then associate with a UvrB molecule to form a $UvrA_2B$ (*13*) or a $UvrA_2B_2$ (*14*, *15*) complex that, in turn, binds to the site of the damaged DNA (*5*, *13*, *16*−*22*) and leads to an ATP-dependent local unwinding around the site of the lesion (*23*, *24*). This conformational change is believed to trigger the dissociation of $UvrA_2$ from the complex. The resulting UvrB−DNA complexes are strongly bent (*25*, *26*), and the DNA is wrapped around the protein (*27*, *28*). Studies of the interactions between the $UvrA_2B$ and DNA substrates suggest that adducted bases are identified by a multilevel recognition process. The recognition by UvrA appears to be based on changes in the local characteristics such as deformations or perturbations of the normal structures of double-stranded damaged DNA, rather than on the recognition of the lesions themselves (*1*, *4*, *10*, *29*). UvrB appears

† This work was supported by NIH/NCI Grant CA 099194 (to N.E.G.) and in part by the Intramural Research Program of the NIH, National Institute of Environmental Health Sciences (to B.V.H.). The racemic diol epoxide *anti*-BPDE was obtained from the National Cancer Institute Carcinogen Reference Standard Repository, supported by the U.S. Public Health Service, National Institutes of Health.

* To whom correspondence should be addressed. Tel: (212) 998-8407. Fax: (212) 998-8421. E-mail: ng1@nyu.edu.

‡ New York University.

§ National Institutes of Health.

|| Slovak Academy of Sciences.

⊥ East Tennessee State University.

# Penn State College of Medicine.

10.1021/bi700294k CCC: $37.00 
Published on Web 05/17/2007

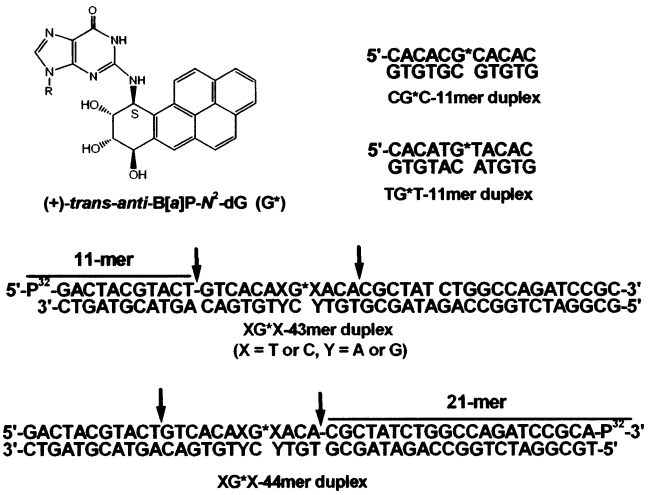


FIGURE 1: Structure of the (+)-*trans*-B[*a*]P-$N^2$-dG adduct and site-specifically modified 11-mer oligonucleotide duplexes. Definition of the 43-mer and 44-mer sequences used in the UvrABC incision and UvrAB binding experiments. The UvrC nuclease incision points of the 5′-end-labeled 43-mer and 3′-end-labeled 44-mer duplexes are shown by the vertical arrows. The sequences of the 11-mer and 21-mer (horizontal bars) of the 5′- and 3′-$^{32}$P-labeled incision fragments, respectively, are also shown.

to provide a second level of damage discrimination that involves a strand separation and hydrophobic stacking interactions via the intercalative insertion of aromatic amino acid residues on the $\beta$-hairpin of UvrB between neighboring base pairs (*19*, *21*, *24*, *27*, *30*−*33*). The UvrC protein interacts with the UvrB molecule in the UvrB−DNA complex to form a pre-incision UvrBC−DNA complex with 4−6 unpaired bases in a bubble-like structure around the site of the lesion (*24*, *34*). This protein complex exhibits an ATP-dependent endonuclease activity (*35*) with an initial 3′-incision at the fourth−fifth phosphodiester bond on the 3′-side of the lesion, followed by a 5′-incision at the eighth phosphodiester bond (*36*, *37*).

The conformations of the (+)-*trans*-B[*a*]P-$N^2$-dG adducts (G*, Figure 1) (*38*) and several stereoisomeric adducts (*39*) in double-stranded DNA have been investigated by NMR methods. The relative efficiencies of incision of DNA sequences containing such B[*a*]P−DNA lesions by mammalian (*40*) and prokaryotic (*5*, *6*, *21*, *41*, *42*) NER proteins have also been studied. The influence of base sequence-context effects on the NER of different bulky adducts has been noted (*5*, *6*, *34*, *42*−*46*). Effects of adduct conformation on NER have been described for stereoisomeric B[*a*]P-$N^2$-dG adducts in the same sequence context (*5*) and *N*-[deoxyguanosin-8-yl]-2-aminofluorene adduct positioned at different sites in a *NarI* mutation hotspot sequence (*47*).

In order to gain a better understanding of the fundamental principles underlying base sequence effects on NER, we investigated the efficiencies of incision catalyzed by the UvrABC system of two DNA duplexes containing identical (+)-*trans*- B[*a*]P-$N^2$-dG adducts embedded in two different sequence contexts. The two sequence contexts were selected in order to maintain the same minor groove conformational motif of the lesion, while changing the thermodynamic stabilities of only the two base pairs flanking this lesion. In one duplex, the lesion G* was flanked on both sides by T and in the other by C (these duplexes are denoted by TG*T and CG*C, respectively; Figure 1). These two types of substrates were selected because the properties of the (+)-*trans*-B[*a*]P-$N^2$-dG adducts have been extensively studied in these base sequence contexts by NMR (*38*, *39*, *48*) and other biophysical techniques (*48*, *49*). A single minor groove conformation is observed, all Watson−Crick base pairs are intact (*38*), and the adduct causes a rigid bend (*49*) in the CG*C sequence context. In contrast, multiple adduct conformations are observed in a TG*T sequence context, a weakening of Watson−Crick base pairing is observed at adduct G* and the two 5′-flanking base pairs, and the site of modification is characterized by a highly flexible bend (*48*, *49*). Theses observations indicate that base pair opening in the immediate vicinity of lesions G* is more facile in the TG*T than in the CG*C sequence context. If local structural deviations from normal base stacking and Watson−Crick base pairing caused by the lesions represent an important recognition element for prokaryotic UvrABC proteins, incisions should be favored in TG*T relative to CG*C sequence contexts, and such an effect can be related to differences in nearest neighbor interactions. This hypothesis was tested using UvrABC proteins from the thermophilic organism *Bacillus caldotenax* (*50*) and from *E. coli*.

## EXPERIMENTAL PROCEDURES

*Preparation of B[a]PDE-Modified Oligonucleotides*. All oligonucleotides were synthesized using the Biosearch Cyclone DNA synthesizer and were purified by standard HPLC protocols. The BPDE-modified oligonucleotides were generated by direct synthesis methods using racemic *anti*-B[*a*]PDE obtained from the National Cancer Institute Carcinogen Reference Repository (NIH, Bethesda, MD). The procedures used and the methods of characterization and verification of adduct stereochemistry were the same as those described earlier (*51*).

The 11-mers were extended to 43-mers by standard ligation methods as described elsewhere (*52*). The 43-mer oligonucleotides were either 5′-end-labeled with [$\gamma$-$^{32}$P] ATP or 3′-end-labeled with 5′-[$\alpha$-$^{32}$P] ddATP (GE Healthcare Bio-Sciences, Piscataway, NJ), thus forming 44-mer oligonucleotides (Figure 1). The 5′-end-labeled substrates were prepared by labeling 5 pmol of the 43-mer oligonucleotides with [$\gamma$-$^{32}$P] ATP using 10 units of T4 polynucleotide kinase in a 10 $\mu$L reaction volume at 37 °C for 1 h. The 3′-end-labeling reactions were conducted by labeling the 43-mer TG*T and CG*C oligonucleotides with 5′-[$\alpha$-$^{32}$P]ddATP at 37 °C for 30 min. The 50 $\mu$L reaction mixture contained 5 pmol of the oligonucleotides, 0.1 mM ddATP, and 50 units of terminal deoxynucleotidyl transferase (calf thymus, GE Healthcare Bio-Sciences, Piscataway, NJ). The reaction was stopped by adding 5 $\mu$L of 0.5 M EDTA solution. The end-labeled 43-mer or 44-mer oligonucleotides were purified using 20% denaturing polyacrylamide gel and then desalted by ethanol precipitation.

*B. caldotenax UvrABC Incision Protocol*. The cloning of *B. caldotenax* UvrA, UvrB, and UvrC genes and the purfication of the proteins have been described in detail elsewhere (*53*). Aliquots of the UvrA, UvrB, and UvrC stock solutions (0.5, 0.8, and 1 $\mu$M, respectively) were stored at −20 °C. Before use, the enzymes were diluted with UvrABC buffer (50 mM Tris-HCl at pH 7.5, 50 mM KCl, 10 mM

$MgCl_2$, 5 mM dithiothreitol, and 1 mM ATP). The buffer and enzymes were kept at 0 °C during the dilution. The diluted enzymes were pre-heated at 55 °C for 5 min to achieve optimal activity and to inactivate possible *E. coli* contaminant nucleases. In the incision assay, the final concentrations employed were 25 nM UvrA, 40 nM UvrB, 50 nM UvrC, and 2 nM oligonucleotide duplex substrates. The reactions were carried out in 40 $\mu$L solutions obtained by mixing 4 $\mu$L of UvrABC buffer, 6 $\mu$L of the diluted UvrA, UvrB, and UvrC solution, 2 $\mu$L of the double-stranded DNA substrate, and 28 $\mu$L of water. After incubation of these solutions for a specified time interval and temperature, the reactions were stopped by adding 1.3 $\mu$L of a 0.1 M EDTA solution to a 6 $\mu$L aliquot of the reaction mixture. The solutions were then centrifuged in a low-vacuum concentrator ("SpeedVac" Model SVC 100, ThermoFisher Scientific, Waltham, MA) at a medium drying rate in order to reduce the volume to less than 2 $\mu$L. The samples were heated at 90 °C for 3 min, then quickly chilled in ice-water, and loaded onto a 20% denaturing polyacrylamide sequencing gel in TBE buffer (0.089 M Tris, 0.089 M sodium borate, and 0.002 M EDTA). The gel was operated at about 55−60 °C. Upon completion of the gel electrophersis run, it was dried and the bands were visualized using a Storm 840 PhosphorImager (GE Healthcare Biosciences, Inc., Piscataway, NJ). The relative radioactivities of the bands were evaluated employing the ImageQuant software of the Storm 840 system.

*E. coli UvrABC Incision Protocol*. The *E. coli* NER proteins were expressed and purified as described elsewhere (*53*). The UvrA, UvrB, and UvrC stock solutions were diluted to concentrations of 0.2, 5, and 2 $\mu$M, respectively, with the UvrABC buffer in 20% glycerol/ $H_2O$ solution. The buffer was pre-chilled to 0 °C before use. As in the case of the experiments with *B. caldotenax*, the DNA substrates were dissolved in UvrABC reaction buffer and pre-heated at 37 °C for 5 min. The diluted UvrA and UvrB solutions were mixed first, and then the UvrC was added with all solutions chilled to −20 °C in a salt-water/ice bath. This mixture of enzymes was then added to the DNA substrate solution. The final incision reaction mixtures contained 10 nM UvrA, 250 nM UvrB, 100 nM UvrC, and 2 nM DNA substrate. The *E. coli* repair reaction was stopped and analyzed in the same manner as the NER reactions with *B. caldotenax*.

*Protein−DNA Binding Experiments by Gel Electrophoretic Mobility Shift Assays*. The binding reactions were performed with 2 nM DNA solutions ($^{32}$P-end-labeled modified strands), 25 nM *B. caldotenax* UvrA, or 40 nM *B. caldotenax* UvrB and 25 nM UvrA (same concentrations of these proteins as in the incision reactions) in 20 $\mu$L of ABC buffer and incubated at 37 °C for 30 min. Glycerol was then added to the solutions (80% v/v), and the reaction mixture was loaded onto a 4% native polyacrylamide gel (29:1). The electrophoresis was performed for 30 min at 4 °C with a current of 50 mA in a vertical mini-gel electrophoresis unit (Hoefer SE 250, 8 × 10 cm) and running buffer (TBE buffer containing 10 mM $MgCl_2$ and 1 mM ATP). The gels were then dried and visualized by autoradiography.

*UV DNA Melting Profiles*. The dissociation of the double-stranded DNA duplexes as a function of temperature was measured by monitoring the UV absorbance of DNA solutions (50 mM sodium phosphate buffer and 100 mM NaCl at pH 7.2) at the DNA absorbance maximum of 260 nm and the B[*a*]P-residue absorbance maximum at 346 nm utilizing a diode array spectrophotometer (Model 8453, Agilent Technologies, Inc., Santa Clara, CA) equipped with a thermostatted cuvette. The melting profiles were generated by plotting the absorbance at a given wavelength as a function of temperature.

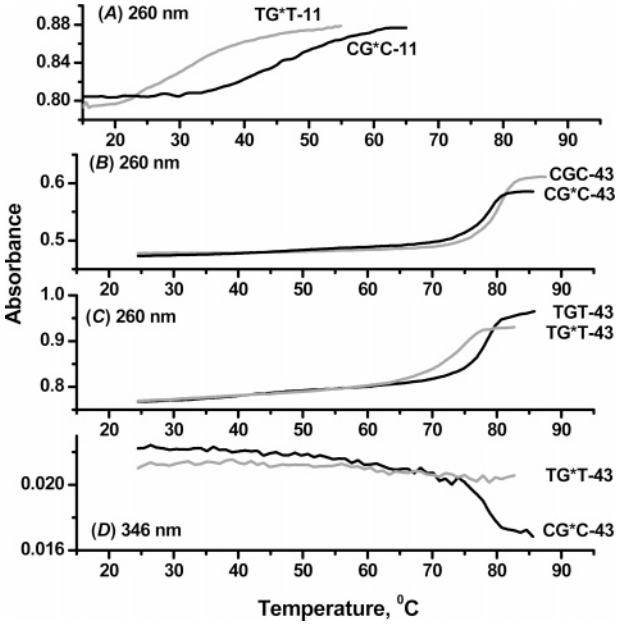


FIGURE 2: (A) Typical UV melting curves of the B[*a*]PDE-modified double-stranded forms of the TG*T-11-mer and CG*C-11-mer oligonucleotide duplexes. The absorbance (260 nm) measurements (10 mm optical path length) were made at ~7 $\mu$M oligonucleotide concentration and 100 mM NaCl and 20 mM sodium phosphate buffer solution at pH 7. The rate of temperature increase was 0.5 degrees/min. Comparisons of UV melting curve profiles of (B) the unmodified CGC- and modified CG*C-43mer duplexes (0.7 $\mu$M) and (C) the unmodified TGT- and TG*T-43-mer duplexes (1 $\mu$M) monitored at 260 nm. (D) Absorbance of the same B[*a*]PDE-modified CG*C- and TG*T-43mer duplexes (~1 $\mu$M) monitored at 346 nm as a function of temperature.

## RESULTS

*UV Melting Profiles and Physical Characteristics of the G* Adducts in CG*C and TG*T Sequences*. The UV (260 nm) melting profiles of the TG*T and CG*C 11-mer oligonucleotide duplexes are shown in Figure 2A. The melting points of the duplexes, $T_m$, were determined from the maxima in the derivatives of plots of the absorbance at 260 nm versus temperature (data not shown). The $T_m$ value of the TG*T-11-mer duplex (30 ± 1 °C) is ~15 degrees lower than the $T_m$ value of the CG*C-11-mer duplex (46 ± 1 °C). This indicates that T:A base pairs flanking the adduct tend to destabilize the TG*T-11-mer duplexes as shown previously by NMR methods (*48*). The $T_m$ values of the TG*T-11-mer and CG*C-11-mer duplex are ~11° and 9°, respectively, lower than those of the respective unmodified TGT- and CGC-11-mer duplexes.

The 11-mer duplexes, however, are too small for the UvrABC incision experiments because the footprints of the UvrA and UvrB proteins bound to damaged DNA duplexes range from 19 to 33 base pairs (*54*). It was therefore necessary to construct the longer 43-mer duplexes depicted in Figure 1. The $T_m$ values of the 43-mer duplexes are significantly higher than those of the 11-mer duplexes (Figure

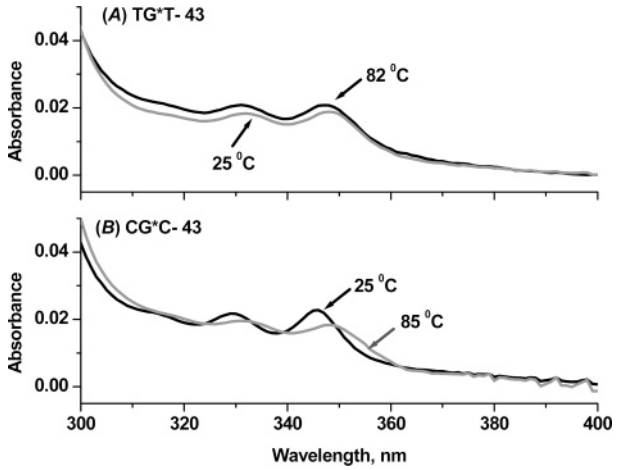


FIGURE 3: UV absorption spectra of the B[*a*]P residues in (A) TG*T-43mer and (B) CG*C-43mer duplexes (same as those in Figure 2) in the 300−400 nm region measured at 25 °C (duplex form, black lines) and >80 °C (denatured form, gray lines).

2B and C). However, effects of the lesions on the thermal stabilities are still observable, especially in the case of the TG*T-43-mer duplex because $T_m = 75.0 \pm 0.9$ °C, about 3−4 degrees lower than the $T_m$ of the unmodified 43-mer duplex (Figure 2C). In contrast, the $T_m$ value of the modified CG*C-43-mer duplex is only slightly lower than the $T_m$ of the unmodified CGC-43-mer duplex (Figure 2B).

The 260 nm UV melting profiles (Figure 2B and C) reflect the melting of the entire duplex but do not provide insights into the local melting characteristics of the (+)-*trans*-B[*a*]P-$N^2$-dG adducts. The pyrene-like B[*a*]P residues exhibit an absorbance in the 300−360 nm region, well outside the absorption band of the DNA (Figure 3), and are highly sensitive to changes in the local environment. At 25 °C, the absorption spectra of the lesions reflect their environment in the double-stranded form with maxima near 346 nm, while at temperatures beyond $T_m$ at 82−85 °C, their absorption spectra are red-shifted and characteristic of a single-stranded environment with maxima near 350 nm (*55*) and a marked decrease in the molar absorption coefficient (Figure 3). Depending on the wavelength of observation, either hyperchromic or hypochromic absorbance changes can be observed as duplexes are formed or as they undergo dissociation (*55*). In the case of the CG*C-43-mer duplex, the absorbance at 346 nm is higher in the duplex than in the single-stranded form, and this absorbance decreases slowly with increasing temperature. A further abrupt decrease is observed in the 75−80 °C region (Figure 2D) near the $T_m$ of 79.4 ± 0.4 °C measured at 260 nm (Figure 2B). In contrast, little change in the absorbance at 346 nm is observed in the case of the TG*T-43-mer duplex in the entire temperature interval (Figures 2D and 3A), suggesting that there is no significant change in the local environment of the pyrenyl ring system as the temperature is increased from 15 °C to ~82 °C.

*Incisions Catalyzed by UvrABC Proteins from B. caldotenax.* Typical gel autoradiograms obtained after the incisions of TG*T-43 and CG*C-43-mer duplexes after different incubation times at temperatures of 37 °C are depicted in Figure 4A. The incision products are the 5′-end-labeled 11-mer oligonucleotides (Figure 1). The single-stranded 43-mer sequences containing the (+)-*trans*-B[*a*]P-$N^2$-dG lesions migrate slower than the unmodified strands (lanes U). In some cases, two bands are observed in the region of the 43-mers at the top of the gels. The upper band disappears when the solutions are extracted with a standard phenol−chloroform solution, which is attributed to protein−DNA complexes (data not shown) that did not affect the quantitation of incision products. At 37 °C, the TG*T-43-mer duplexes are incised with greater initial rates than the CG*C-11-mer duplexes (Figure 4B). In this example, the initial rates of incision are 2.6 ± 0.15 times greater at 37 °C in the case of the TG*T-43-mer than in the case of the CG*C-43-mer duplexes. Repeated experiments with different preparations of UvrABC over a period of 3 years consistently yielded values for this ratio in the range of 2.3 ± 0.3.

The thermophilic UvrABC proteins are active and stable up to 55−60 °C (*50*, *53*), and it was therefore possible to obtain reproducible incision results in the range of 37−55 °C. The temperature dependence of the initial incision rates was measured for both the TG*T- and CG*C-43-mer duplexes, and typical gel electrophoresis results are shown in Supporting Information, Figure S1. The results are plotted in Figure 4C according to the Arrhenius equation $k = A\exp[-E_a/RT]$ in the semilogarithmic representation, where $k$ is the rate constant (proportional to the measured initial incision rates), $E_a$ is the activation energy, and $A$ is the pre-exponential factor. These Arrhenius plots are linear within experimental error, and the activation energies deduced from the slopes of these plots are $E_a = 27.0 \pm 1.5$ and $23.4 \pm 1.0$ kcal/mol for the CG*C- and TG*T-43-mer duplexes, respectively.

We next considered whether base sequence effects on incision rates are also observable with UvrABC proteins from the non-thermophilic *E. coli*. The time course of typical incision reactions of 5′-end-labeled TG*T-43-mer and CG*C-43-mer duplexes at 37 °C are shown in the gel autoradiogram in Figure 5A, and the same 11-mer 5′-end-labeled incision products are observed, as in the case of the *B. caldotenax* experiments. The fraction of 43-mer duplexes incised is linear up to about 30 min (Figure 5B). The difference in the incision rates catalyzed by the *E. coli* UvrABC proteins exhibits the same trend, as in the case of incisions catalyzed by UvrABC from *B. caldotenax.* However, the initial incision rates of TG*T-43-mer duplexes are only ~1.7 ± 0.1 times greater than the incision rates of the CG*C-43-mer duplexes. We also examined the incision rates on the 3′-sides of the lesions by labeling the modified oligonucleotides at their 3′-ends, and a typical gel autoradiogram is shown in Supporting Information, Figure S2. The fractions of 3′-incised 44-mers, as evidenced by the appearance of the expected 21-mer 3′-incision products (Figure 1), are similar to the fractions of 5′-incision products (Figure 5B). This is consistent with the previously established notion that the 3′-incision precedes the 5′-incision when lesions are excised by *E. coli* UvrABC proteins (*36*). We note in passing that in contrast to the efficient 3′-incisions observed in the case of the proteins derived from *E. coli*, the 3′-incision was significantly less efficient in the case of the UvrC protein derived from *B. caldotenax*, as discussed by Jiang et al. (*53*). These results indicated that the 3′-incision catalyzed by the *B. caldotenax* UvrC proteins does not need to precede the 5′-incision as in the case of the incisions of damaged DNA catalyzed by UvrABC proteins from *E. coli* (*36*).

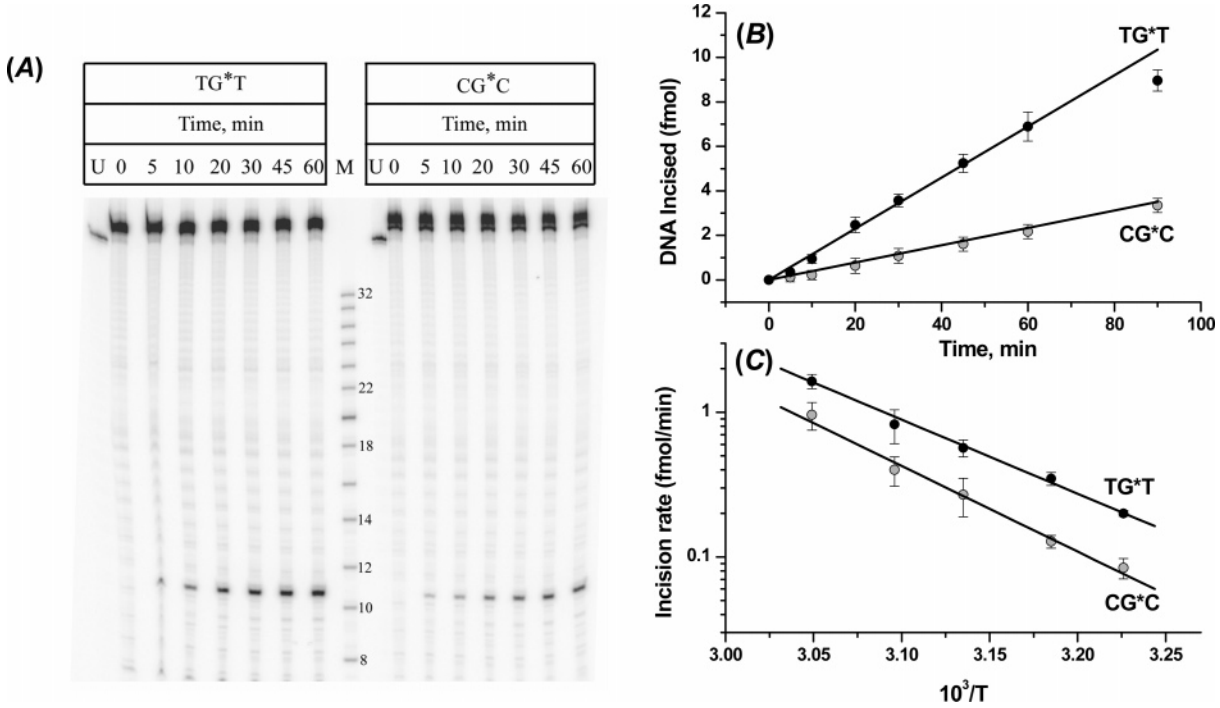


FIGURE 4: Time and temperature dependence of incisions determined with either TG*T-43-mer or CG*C-43-mer oligonucleotide duplexes (2 nM). (A) Typical gel autoradiograms of 5′-end-labeled incision products (11-mers) appearing after incubation with *B. caldotenax* 25 nM UvrA, 40 nM UvrB, and 50 nM UvrC at 37 °C as a function of incubation time. U: unmodified TGT-43-mer or CGC-43-mer oligonucleotides. M: ladder of oligonucleotide markers 8, 10, 12, 14.....30, 32 bases in length. (B) Example of the time course of incisions at 37 °C; the data points represent the average of 4−6 independent experiments. The error bars indicate the standard deviations. (C) Arrhenius plots of the initial incision rates as a function of temperature. The activation energies determined from the slopes of the best-fit straight lines are $E_a = 23.4 \pm 1.0$ kcal/mol for the TG*T-43-mer and $E_a = 27.0 \pm 2.0$ kcal/mol for the CG*C-43-mer duplexes. The averages were calculated from 3 to 4 independent experiments, and the error bars denote the standard deviations of the measurements. The incubation times at the different temperatures were adjusted to maintain incision yields below 20% in all cases.

*Binding of UvrA and UvrB Proteins to the TG*T- and CG*C-43-mer Duplexes*. The possibility that the difference in incision rates of the TG*T and CG*C duplexes is due to the recognition of the damaged sequences by UvrA or a combination of UvrA and UvrB proteins was explored. Autoradiograms of typical native gel experiments conducted with proteins from *B. caldotenax* are shown in Figure 6. The UvrA and UvrB concentrations were the same as those utilized in the incision experiments, except that UvrC was absent. The bands shown in Figure 6 were assigned according to the identifications described earlier (*31*, *56*). The formation of $UvrA_2$−DNA complexes ([UvrA] = 25 nM, [UvrB] = 0) is distinctly greater in the case of the TG*T-43-mer than in the case of the CG*C-43-mer duplexes by a factor 1.7 ± 0.2 (Figure 7A). The concentrations of the $UvrA_2B$ complexes are also greater by a factor of 1.7 ± 0.4 in the TG*T-43-mer than in the case of the CG*C-43-mer duplexes. However, the levels of UvrB−DNA complexes are more similar to one another, although still greater in the case of TG*T by a factor of 1.3 ± 0.2 (Figure 7A). Additional details are provided in Supporting Information. The dependence of $UvrA_2$−DNA complex formation on the concentration of UvrA is depicted in Figure 7B. The shapes of the curves are sigmoidal, reflecting the complexity of coupled equilibria that include the dimerization of UvrA molecules. The apparent $K_{d(50)}$ values (UvrA concentrations needed to bind 50% of the DNA molecules) are 59 ± 3 and 83 ± 4 nM for the TG*T- and CG*C-43-mer duplexes, respectively. However, the ratios of initial incision rates (TG*T/CG*C) are independent of the UvrA concentrations in the range of 25−200 nM at 37 or 55 °C (Figure S3, Supporting Information).

## DISCUSSION

Prokaryotic nucleotide excision repair proteins recognize and excise a variety of structurally distinct lesions (*4*, *57*). It has been proposed that the UvrABC system probes the distortions of the DNA helix associated with the loss of base stacking and Watson−Crick hydrogen bonding that causes local destabilization of the double-stranded DNA at the site of bulky lesions (*10*). Naegeli and co-workers advanced the related concept that mammalian NER proteins probe the loss of hydrogen bonding and the local structural disorder caused by bulky DNA adducts (*58*). Because bulky lesions such as the (+)-*trans*-B[*a*]P-$N^2$-dG adducts are known to destabilize DNA duplexes (*59*), we postulated that the degree of local disorder and destabilization might also depend on the nature of the bases flanking the lesions. We tested this hypothesis by replacing C:G base pairs flanking the adduct G* by the thermodynamically less stable (*60*, *61*) T:A base pairs and by measuring the incision rates catalyzed by UvrABC nuclease. The UvrABC proteins from the thermophilic organism *B. caldotenax* (*53*) are suitable for probing such effects because incision kinetics can be studied at different temperatures, up to ∼55−60 °C (*50*).

*Sequence Effects on Local Structural Order and the Conformational Characteristics of B[a]P-$N^2$-dG Adducts of TG*T- and CG*C-11-mer Duplexes.* Although a single minor groove adduct conformation with the B[*a*]P residue on the

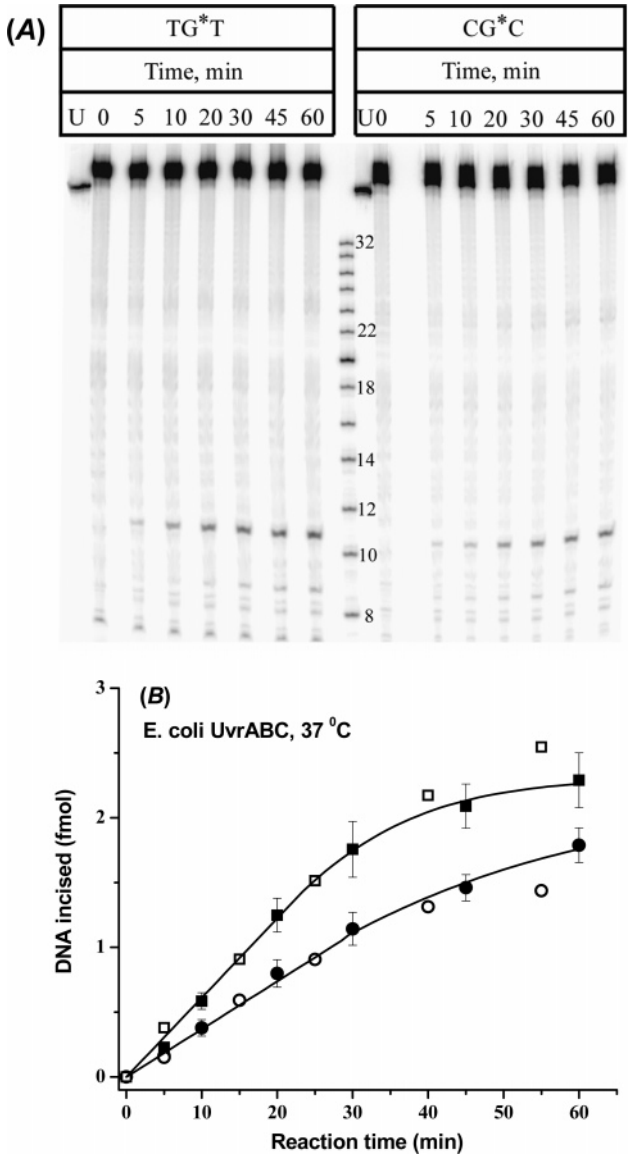


FIGURE 5: (A) Typical gel autoradiogram of incision products (11-mers) after incubation of UvrABC proteins from *E. coli* with either TG*T-43mer or CG*C-43-mer oligonucleotide duplexes (2 nM) at 37 °C. U: unmodified TGT-43mer or CGC-43mer oligonucleotides. A ladder of oligonucleotide markers 8, 10, 12, 14.....32 bases long is shown in the middle. (B) Time course (min) of incisions at 37 °C catalyzed by UvrABC proteins from *E. coli* and 5′-end-labeled TG*T-43mer (■) and CG*C-43mer (●) duplexes and 3′-end-labeled duplexes (□ and ○), respectively.

5′-side of the modified guanine is observed in the CG*C sequence contexts with intact Watson−Crick base pairing in the flanking base pairs (*38*), the same adduct in a TG*T sequence context has entirely different properties. The B[*a*]P residue exhibits multiple conformations on the NMR time scale, and base pairing is weakened within the trinucleotide sequence 5′-d(...ATG*...)•3′-d(...TAC...). The imino proton resonances associated with normal B−DNA Watson−Crick base pairs were not observed in this region of the duplex (*48*). The enhanced exchange of imino protons with the solvent (*62*) indicates a higher frequency of base pair opening events in this segment of the duplex. A less pronounced destabilization of local base pairs caused by the same (+)-*trans*-B[*a*]P-$N^2$-dG adducts has also been reported in a TG*C sequence context (*63*). The local destabilization of base pairs on the 5′-side of the adduct in the TG*T

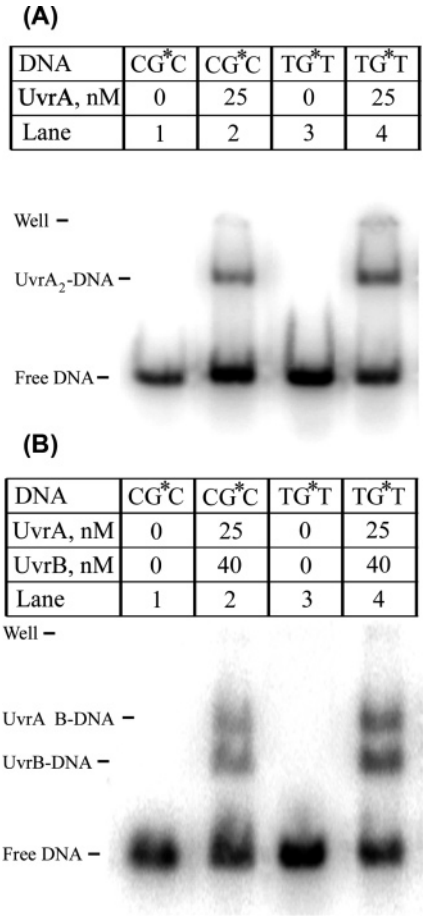


FIGURE 6: Typical autoradiograms of gels (4.5% polyacrylamide) obtained after incubation of *B. caldotenax* (A) UvrA (25 nM), or (B) UvrA (25 nM) and UvrB (40 nM) with either the CG*C-43-mer or the TG*T-43mer (2 nM) duplex incubated at 37 °C.

duplexes is consistent with the orientational preference of the bulky pyrenyl residue on the 5′-side of the modified guanine residue G* (*39*, *48*, *64*), and there is no NMR evidence for the existence of an intercalated structure. Circularization and gel electrophoresis studies of the TG*T-11-mer duplexes further indicate that there are significant differences in the local environments of the TG*T and CG*C duplexes. A flexible locus of bending is observed at the site of the lesion in TG*T, which allows for the formation of circular DNA molecules as small as 77 base pairs in size (*48*). In contrast to the highly flexible TG*T-11-mer duplex sequence context, the CG*C-11-mer duplexes exhibit a rigid bend (*49*) as well as a greater average extent of bending (*65*).

*Probing the Local B[a]P-$N^2$-dG Adduct Environment in TG*T- and CG*C-43-mer Duplexes*. Studies of the melting and spectroscopic characteristics of the TG*T and CG*C complexes suggest that the sequence effects on the local environment of the (+)-*trans*-B[*a*]P-$N^2$-dG adducts observed in the 11-mer duplexes persist in the 43-mer duplexes (Figure 2). In general, the effects of base sequence on the melting characteristics of double-stranded DNA can be estimated from consideration of the free energy terms defining the interactions between successive dinucleotide steps (*59*). The 5′-TG or 5′-GT dinucleotide steps in double-stranded oligonucleotides are thermodynamically less stable than the 5′-CG or 5′-GC dinucleotide steps (*60*). The base sequence effects on $T_m$ are predominantly enthalpic in nature (*60*) and arise mainly from differences in base−base stacking interac-

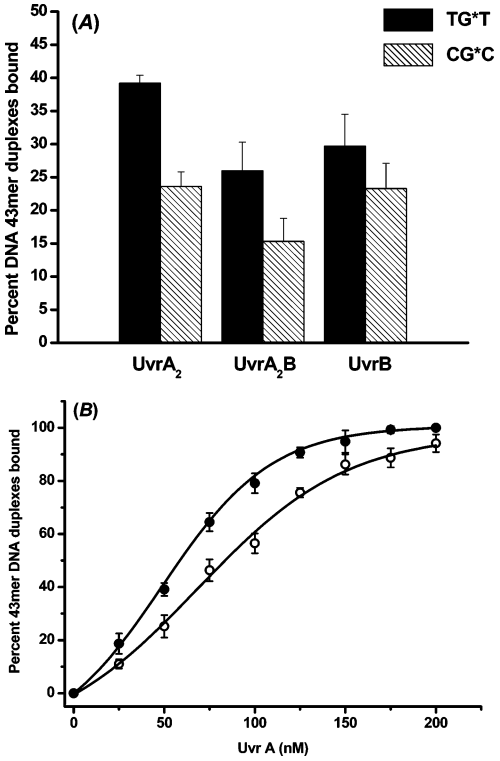


FIGURE 7: (A) Formation of $UvrA_2$−DNA complexes (average of four experiments as in Figure 6A with standard deviations) and $UvrA_2B$− and UvrB−DNA complexes (average of four experiments as in Figure 6B) incubated at 37 °C. Black bars, TG*T-43-mer duplexes; hatched bars, CG*C-43-mer duplexes. (B) Fraction of TG*T-43-mer (●) and CG*C-43mer (○) duplexes (2 nM) bound to $UvrA_2$ proteins in buffer solution in 4% native polyacrylamide gel (see Experimental Procedures for details).

tions (*66*). Thus the observed lower $T_m$ values of the TG*T-11-mer duplexes as compared with those of the CG*C-11-mer (Figures 2A) are consistent with the thermodynamic properties of these two duplexes.

The simultaneous sharp changes in the absorbances at 260 and 347 nm of the CG*C-43-mer duplexes in the vicinity of the $T_m$ temperature indicate that the distinct minor groove conformation of the (+)-*trans*-B[*a*]P-$N^2$-dG adducts is maintained until the entire duplex melts in a cooperative manner (Figure 2B and D). However, in the case of the TG*T-43-mer duplex, the lack of change of the absorbance at 346 nm as a function of temperature is consistent with the absence of a distinct minor groove binding site and the exposure of the B[*a*]P residue to solvent in the entire temperature interval studied. These result are consistent with the enhanced flexibility and local destabilization of the two base pairs flanking the adduct of the 5′-side at ambient temperatures (*48*) and with the apparent solvent exposure of the B[*a*]P residue of G* in the TG*T-43-mer duplex.

Taken together, these physicochemical studies of the properties of oligonucleotide duplexes with single, identical (+)-*trans*-B[*a*]P-$N^2$-dG adducts point to weaker base pairing/base stacking interactions in the TG*T than in the CG*C sequence context. The highly flexible bend in the TG*T sequence context suggests a greater frequency of base pair opening events (*48*) because bending of the double helix and base pair opening are coupled to one another (*67*). These notions are consistent with the experimentally observed multiple adduct conformations in TG*T sequence contexts (*48*) and a single conformation in CG*C sequence contexts (*38*). Our results indicate that the UvrABC proteins can sense sequence-dependent differences in base pair opening dynamics and the accompanying greater local disorder in the TG*T sequence context at 37 °C, that is, at temperatures that are significantly lower than the $T_m$ of the overall 43-mer duplex (Figure 2B and C).

*Base Sequence and Temperature Effects on Incisions Catalyzed by UvrABC Nuclease.* The incision efficiencies increase as a function of temperature, and the linear Arrhenius plots (Figure 4C) suggest that there are no abrupt changes in the conformation of the protein that affect the incision of the damaged DNA strand. Because the measured incisions are a result of a complex series of steps, it is difficult to attribute specific molecular events to the measured activation energies. The proteins and the DNA substrates are likely to contribute to the observed temperature dependence of incision rates.

The activities of thermophilic enzymes increase with temperature. Our measured activation energies in the range of 23−28 kcal/mol are near the higher range of values characterizing the temperature dependence of catalytic rate constants of some other thermophilic enzymes that range from ∼5−24 kcal/mol (*68*−*71*). It is widely accepted that the remarkable activities of thermophilic enzymes result from a conformational rigidity at ambient temperatures with the substrate oriented in unreactive configurations. As the temperature is raised, the electrostatic and other interactions that stabilize the unproductive protein conformations are weakened, resulting in a greater flexibility and thus a greater probability of achieving a configuration that favors the formation of the transition state (*72*, *73*).

The difference in activation energies, although small, is remarkable, showing that the DNA substrate contributes to the measured activation barrier. The activation energy is lower by 3.6 ± 1.8 kcal/mol in the case of the TG*T duplex, thus indicating that the thermodynamically less stable T:A base pairs and weaker nearest neighbor base stacking interactions (*60*, *66*) contribute to the lowering of the reaction barrier in the TG*T case. It has been suggested that UvrB binds to DNA by inserting a β-hairpin between two partially unwound strands of the DNA in the pre-incision complex (*27*, *74*), thus disrupting 4−6 base pairs (*33*). Similar β-hairpin motifs have been observed in the crystal structures of the UvrB protein from *B. caldotenax* and the thermophile *Thermus thermophilus* (*75*, *76*). Sequence homologies of these UvrB proteins with UvrB from *E. coli* suggest that a similar DNA binding hairpin motif may also be found in the latter (*32*). The insertion of the β-hairpins into double-stranded DNA involves the unstacking and disruption of Watson−Crick hydrogen bonding that involves significant costs in energy (*60*, *61*). The relevance of base stacking interactions to DNA repair has been discussed recently (*77*). Raising the temperature from 37 to 55 °C causes a greater flexibility of the DNA substrate. Such temperature-dependent dynamics have been demonstrated by observations of a gradual loss of the imino-proton NMR resonances due to exchange with solvent at temperatures well below the $T_m$ of the DNA duplexes and the enhancement of base pair opening rates in oligonucleotide duplexes as the temperature is increased (*78*). Indeed, it has been shown using the fluorescence of 2-aminopurine, that the unstacking of nucleobases

and the extrusion or flipping of the 3′-nucleotide flanking a cholesterol lesion is an important step governing incisions catalyzed by the *E. coli* UvrABC nuclease system (*79*). A recent cocrystal structure of UvrB bound to DNA substrate containing a three base pair duplex and three base single strand junction supports these fluorescence studies. The structure demonstrated that the $\beta$-hairpin of UvrB is clearly inserted between the two strands with significant base stacking interactions between Tyr96 and the base pair 5′ to the flipped out base (*33*). The lower enthalpies (*60*, *61*) and free energies (*66*) of base stacking interactions in the TG*T sequence context should favor the extrusion of a 3′-flanking thymine relative to extrusion of cytosine in the CG*C context. The smaller activation energy and the enhanced incision rates observed experimentally in the case of the TG*T-43-mer duplex are consistent with these considerations.

*Binding of UvrA and UvrB to TG*T- and CG*C-43-mer Duplexes at 37 °C.* As a first step toward understanding the basis of the base sequence effects on incision rates observed at 37 °C, we investigated the binding affinities of UvrA or UvrA plus UvrB to the TG*T- and CG*C-43-mer duplexes when both are present in solution at concentrations identical to those used in the incision experiments (Figures 6 and 7A). The formation of $UvrA_2$ (Figure 7B) and $UvrA_2B$ complexes (Figures 6B and 7A) is distinctly greater in the case of the TG*T- than the CG*C-43-mer duplexes. This observation suggests that the $UvrA_2$- and $UvrA_2B$-damaged DNA complexes, which are involved in the initial recognition step of DNA damage associated with bulky lesions, depend on base sequence context (Figures 6 and 7). Overall, the sequence dependence of $UvrA_2$ and $UvrA_2B$−DNA complex formation (Figures 6 and 7) is consistent with the notion that the UvrAB proteins recognize the local distortions in the DNA structure that entail a base sequence-dependent weakening of base pairing and base stacking interactions (*10*). However, the sequence-dependent $UvrA_2$−TG*T and CG*C binding constants alone (Figure 7B) cannot explain the differences in incision efficiencies (Figure 5). The ratios of TG*T/CG*C initial incision rates are insensitive to the UvrA concentration, even at saturating conditions of UvrA binding at 200 nM (Figure S3, Supporting Information). These results indicate that the differences in initial incision rates are not simply proportional to the fractions of DNA molecules initially bound to $UvrA_2$ before UvrB binding occurs.

The concentration of $UvrA_2B$−DNA complexes is sequence-dependent and observable at UvrA concentrations up to 45 nM under conditions that are otherwise similar to those of the incision experiments (Figure S4, Supporting Information). However, smaller effects of base sequence context are observed on the formation of UvrB−DNA complexes (Figure 7A), especially at UvrA concentrations approaching 45 nM (Figure S4, Supporting Information). These results are consistent with the suggestions that UvrA is essential for bending and opening the DNA duplex at the site of the lesion, thus facilitating the insertion of the UvrB $\beta$-hairpin into the duplex once it has been opened by UvrA (*33*, *79*).

*Summary and Conclusions.* During prokaryotic nucleotide excision repair, damage detection and commitment to incision is believed to follow two tiers of recognition: (1) UvrA provides the first level of detection, (2) while UvrB verifies the damaged strand and provides a second level of detection (*3*). The three-dimensional structure of UvrB from *B. caldotenax* suggests that this protein uses a helicase fold to process damaged DNA into a stable pre-incision complex using a padlock-like mode of binding in which a $\beta$-hairpin is inserted between the two strands of the DNA duplex in the vicinity of the damaged nucleobase (*32*). The insertion of the $\beta$-hairpin requires a local unstacking of DNA bases that results in the apparent extrusion or base flipping of a nucleobase flanking the lesion site (*33*, *79*). The ease of separation of the two DNA strands is likely to depend on base sequence context because the interactions between neighboring base pairs are base sequence dependent (*59*, *60*). The greater incision efficiencies observed in the case of identical (+)-*trans*-B[*a*]P-$N^2$-dG lesions embedded in TG*T as compared to CG*C sequence contexts in otherwise identical duplexes is consistent with this model and the greater structural disorder in the TG*T duplex sequence context observed by NMR methods (*48*).

## ACKNOWLEDGMENT

We gratefully acknowledge the contributions of Z. Ping to the synthesis of some of the templates used in this work. We are grateful to Professor S. Broyde for stimulating discussions and to N. Goosen for advice on the protein−DNA binding gel electrophoresis experiments.

## SUPPORTING INFORMATION AVAILABLE

Examples of incision experiments at different temperatures, typical autoradiogram of incision products, ratios of initial incision rates measured at different UvrA concentrations, and dependence of the $UvrA_2$−DNA, free DNA, and $UvrB_2$−DNA complexes as a function of UvrA concentration. This material is available free of charge via the Internet at http://pubs.acs.org.

## REFERENCES

1. Sancar, A. (1996) DNA excision repair, *Annu. Rev. Biochem. 65*, 43−81.
2. Wood, R. D. (1999) DNA damage recognition during nucleotide excision repair in mammalian cells, *Biochimie 81*, 39−44.
3. Van Houten, B., Croteau, D. L., Dellavecchia, M. J., Wang, H., and Kisker, C. (2005) 'Close-fitting sleeves': DNA damage recognition by the UvrABC nuclease system, *Mutat. Res. 577*, 92−117.
4. Van Houten, B. (1990) Nucleotide excision repair in *Escherichia coli*, *Microbiol. Rev. 54*, 18−51.
5. Zou, Y., Liu, T. M., Geacintov, N. E., and Van Houten, B. (1995) Interaction of the UvrABC nuclease system with a DNA duplex containing a single stereoisomer of dG-(+)- or dG-(-)-anti-BPDE, *Biochemistry 34*, 13582−13593.
6. Hoare, S., Zou, Y., Purohit, V., Krishnasamy, R., Skorvaga, M., Van Houten, B., Geacintov, N. E., and Basu, A. K. (2000) Differential incision of bulky carcinogen-DNA adducts by the UvrABC nuclease: comparison of incision rates and the interactions of Uvr subunits with lesions of different structures, *Biochemistry 39*, 12252−12261.
7. Naegeli, H., and Geacintov, N. E., Ed. (2005) *The Carcinogenic Effects of Polycyclic Aromatic Hydrocarbons*, Imperial College, London, England.
8. Phillips, D. H. (1983) Fifty years of benzo(a)pyrene, *Nature 303*, 468−472.
9. Szeliga, J., and Dipple, A. (1998) DNA adduct formation by polycyclic aromatic hydrocarbon dihydrodiol epoxides, *Chem. Res. Toxicol. 11*, 1−11.
10. Van Houten, B., and Snowden, A. (1993) Mechanism of action of the *Escherichia coli* UvrABC nuclease: clues to the damage recognition problem, *BioEssays 15*, 51−59.

11. Petit, C., and Sancar, A. (1999) Nucleotide excision repair: from *E. coli* to man, *Biochimie 81*, 15−25.
12. Mazur, S. J., and Grossman, L. (1991) Dimerization off *Escherichia coli* UvrA and its binding to undamaged and ultraviolet light damaged DNA, *Biochemistry 30*, 4432−4443.
13. Orren, D. K., and Sancar, A. (1990) Formation and enzymatic properties of the UvrB.DNA complex, *J. Biol. Chem. 265*, 15796−15803.
14. Verhoeven, E. E., Wyman, C., Moolenaar, G. F., and Goosen, N. (2002) The presence of two UvrB subunits in the UvrAB complex ensures damage detection in both DNA strands, *EMBO J. 21*, 4196−4205.
15. Moolenaar, G. F., Schut, M., and Goosen, N. (2005) Binding of the UvrB dimer to non-damaged and damaged DNA: residues Y92 and Y93 influence the stability of both subunits, *DNA Repair 4*, 699−713.
16. Bertrand-Burggraf, E., Selby, C. P., Hearst, J. E., and Sancar, A. (1991) Identification of the different intermediates in the interaction of (A)BC excinuclease with its substrates by DNase I footprinting on two uniquely modified oligonucleotides, *J. Mol. Biol. 219*, 27−36.
17. Seeberg, E., and Fuchs, R. P. (1990) Acetylaminofluorene bound to different guanines of the sequence -GGCGCC- is excised with different efficiencies by the UvrABC excission nuclease in a pattern not correlated to the potency of mutation induction, *Proc Natl. Acad. Sci. U.S.A. 87*, 191−194.
18. Visse, R., de Ruijter, M., Moolenaar, G. F., and van de Putte, P. (1992) Analysis of UvrABC endonuclease reaction intermediates on cisplatin-damaged DNA using mobility shift gel electrophoresis, *J. Biol. Chem. 267*, 6736−6742.
19. Skorvaga, M., DellaVecchia, M. J., Croteau, D. L., Theis, K., Truglio, J. J., Mandavilli, B. S., Kisker, C., and Van Houten, B. (2004) Identification of residues within UvrB that are important for efficient DNA binding and damage processing, *J. Biol. Chem. 279*, 51574−51580.
20. Truglio, J. J., Croteau, D. L., Skorvaga, M., DellaVecchia, M. J., Theis, K., Mandavilli, B. S., Van Houten, B., and Kisker, C. (2004) Interactions between UvrA and UvrB: the role of UvrB's domain 2 in nucleotide excision repair, *EMBO J. 23*, 2498−2509.
21. Zou, Y., Ma, H., Minko, I. G., Shell, S. M., Yang, Z., Qu, Y., Xu, Y., Geacintov, N. E., and Lloyd, R. S. (2004) DNA damage recognition of mutated forms of UvrB proteins in nucleotide excision repair, *Biochemistry 43*, 4196−4205.
22. DellaVecchia, M. J., Croteau, D. L., Skorvaga, M., Dezhurov, S. V., Lavrik, O. I., and Van Houten, B. (2004) Analyzing the handoff of DNA from UvrA to UvrB utilizing DNA-protein photoaffinity labeling, *J. Biol. Chem. 279*, 45245−45256.
23. Oh, E. Y., and Grossman, L. (1987) Helicase properties of the *Escherichia coli* UvrAB protein complex, *Proc. Natl. Acad. Sci. U.S.A. 84*, 3638−3642.
24. Zou, Y., and Van Houten, B. (1999) Strand opening by the UvrA(2)B complex allows dynamic recognition of DNA damage, *EMBO J. 18*, 4889−4901.
25. Oh, E. Y., and Grossman, L. (1986) The effect of *Escherichia coli* Uvr protein binding on the topology of supercoiled DNA, *Nucleic Acids Res. 14*, 8557−8571.
26. Shi, Q., Thresher, R., Sancar, A., and Griffith, J. (1992) Electron microscopic study of (A)BC excinuclease. DNA is sharply bent in the UvrB-DNA complex, *J. Mol. Biol. 226*, 425−432.
27. Theis, K., Chen, P. J., Skorvaga, M., Van Houten, B., and Kisker, C. (1999) Crystal structure of UvrB, a DNA helicase adapted for nucleotide excision repair, *EMBO J. 18*, 6899−6907.
28. Verhoeven, E. E., Wyman, C., Moolenaar, G. F., Hoeijmakers, J. H., and Goosen, N. (2001) Architecture of nucleotide excision repair complexes: DNA is wrapped by UvrB before and after damage recognition, *EMBO J. 20*, 601−611.
29. Zou, Y., Bassett, H., Walker, R., Bishop, A., Amin, S., Geacintov, N. E., and Van Houten, B. (1998) Hydrophobic forces dominate the thermodynamic characteristics of UvrA- DNA damage interactions, *J. Mol. Biol. 281*, 107−119.
30. Hsu, D. S., Kim, S. T., Sun, Q., and Sancar, A. (1995) Structure and function of the UvrB protein, *J. Biol. Chem. 270*, 8319−8327.
31. Skorvaga, M., Theis, K., Mandavilli, B. S., Kisker, C., and Van Houten, B. (2002) The beta-hairpin motif of UvrB is essential for DNA binding, damage processing, and UvrC-mediated incisions, *J. Biol. Chem. 277*, 1553−1559.
32. Theis, K., Skorvaga, M., Machius, M., Nakagawa, N., Van Houten, B., and Kisker, C. (2000) The nucleotide excision repair protein UvrB, a helicase-like enzyme with a catch, *Mutat. Res. 460*, 277−300.
33. Truglio, J. J., Karakas, E., Rhau, B., Wang, H., DellaVecchia, M. J., Van Houten, B., and Kisker, C. (2006) Structural basis for DNA recognition and processing by UvrB, *Nat. Struct. Mol. Biol. 13*, 360−364.
34. Zou, Y., Shell, S. M., Utzat, C. D., Luo, C., Yang, Z., Geacintov, N. E., and Basu, A. K. (2003) Effects of DNA adduct structure and sequence context on strand opening of repair intermediates and incision by UvrABC nuclease, *Biochemistry 42*, 12654−12661.
35. Zou, Y., Walker, R., Bassett, H., Geacintov, N. E., and Van Houten, B. (1997) Formation of DNA repair intermediates and incision by the ATP-dependent UvrB-UvrC endonuclease, *J. Biol. Chem. 272*, 4820−4827.
36. Verhoeven, E. E., van Kesteren, M., Moolenaar, G. F., Visse, R., and Goosen, N. (2000) Catalytic sites for 3′ and 5′ incision of *Escherichia coli* nucleotide excision repair are both located in UvrC, *J. Biol. Chem. 275*, 5120−5123.
37. Truglio, J. J., Rhau, B., Croteau, D. L., Wang, L., Skorvaga, M., Karakas, E., DellaVecchia, M. J., Wang, H., Van Houten, B., and Kisker, C. (2005) Structural insights into the first incision reaction during nucleotide excision repair, *EMBO J. 24*, 885−894.
38. Cosman, M., de los Santos, C., Fiala, R., Hingerty, B. E., Singh, S. B., Ibanez, V., Margulis, L. A., Live, D., Geacintov, N. E., Broyde, S., et al. (1992) Solution conformation of the major adduct between the carcinogen (+)-anti-benzo[a]pyrene diol epoxide and DNA, *Proc. Natl. Acad. Sci. U.S.A. 89*, 1914−1918.
39. Geacintov, N. E., Cosman, M., Hingerty, B. E., Amin, S., Broyde, S., and Patel, D. J. (1997) NMR solution structures of stereoisometric covalent polycyclic aromatic carcinogen-DNA adduct: principles, patterns, and diversity, *Chem. Res. Toxicol. 10*, 111−146.
40. Hess, M. T., Gunz, D., Luneva, N., Geacintov, N. E., and Naegeli, H. (1997) Base pair conformation-dependent excision of benzo[a]pyrene diol epoxide-guanine adducts by human nucleotide excision repair enzymes, *Mol. Cell. Biol. 17*, 7069−7076.
41. Tang, M. S., Pierce, J. R., Doisy, R. P., Nazimiec, M. E., and MacLeod, M. C. (1992) Differences and similarities in the repair of two benzo[a]pyrene diol epoxide isomers induced DNA adducts by uvrA, uvrB, and uvrC gene products, *Biochemistry 31*, 8429−8436.
42. Zou, Y., Luo, C., and Geacintov, N. E. (2001) Hierarchy of DNA damage recognition in *Escherichia coli* nucleotide excision repair, *Biochemistry 40*, 2923−2931.
43. Delagoutte, E., Fuchs, R. P., and Bertrand-Burggraf, E. (2002) The isomerization of the UvrB-DNA preincision complex couples the UvrB and UvrC activities, *J. Mol. Biol. 320*, 73−84.
44. Delagoutte, E., Bertrand-Burggraf, E., Dunand, J., and Fuchs, R. P. (1997) Sequence-dependent modulation of nucleotide excision repair: the efficiency of the incision reaction is inversely correlated with the stability of the pre-incision UvrB-DNA complex, *J. Mol. Biol. 266*, 703−710.
45. Mekhovich, O., Tang, M., and Romano, L. J. (1998) Rate of incision of N-acetyl-2-aminofluorene and N-2-aminofluorene adducts by UvrABC nuclease is adduct- and sequence-specific: comparison of the rates of UvrABC nuclease incision and protein-DNA complex formation, *Biochemistry 37*, 571−579.
46. Luo, C., Krishnasamy, R., Basu, A. K., and Zou, Y. (2000) Recognition and incision of site-specifically modified C8 guanine adducts formed by 2-aminofluorene, N-acetyl-2-aminofluorene and 1-nitropyrene by UvrABC nuclease, *Nucleic Acids Res. 28*, 3719−3724.
47. Meneni, S., Shell, S. M., Zou, Y., and Cho, B. P. (2007) Conformation-specific recognition of carcinogen-DNA adduct in *Escherichia coli* nucleotide excision repair, *Chem. Res. Toxicol. 20*, 6−10.
48. Xu, R., Mao, B., Amin, S., and Geacintov, N. E. (1998) Bending and circularization of site-specific and stereoisomeric carcinogen-DNA adducts, *Biochemistry 37*, 769−778.
49. Tsao, H., Mao, B., Zhuang, P., Xu, R., Amin, S., and Geacintov, N. E. (1998) Sequence dependence and characteristics of bends induced by site- specific polynuclear aromatic carcinogen-deoxyguanosine lesions in oligonucleotides, *Biochemistry 37*, 4993−5000.
50. Jiang, G. H., Skorvaga, M., Croteau, D. L., Van Houten, B., and States, J. C. (2006) Robust incision of benoz[a]pyrene-7,8-

dihyrodiol-9,10-epoxide-DNA adducts by a recombinant thermoresistant interspecies combination UvrABC endonuclease system, *Biochemistry 45*, 7834−7843.
51. Geacintov, N. E., Cosman, M., Mao, B., Alfano, A., Ibanez, V., and Harvey, R. G. (1991) Spectroscopic characteristics and site I/site II classification of cis and trans benzo[a]pyrene diolepoxide enantiomer-guanosine adducts in oligonucleotides and polynucleotides, *Carcinogenesis 12*, 2099−2108.
52. Zhuang, P., Kolbanovskiy, A., Amin, S., and Geacintov, N. E. (2001) Base sequence dependence of in vitro translesional DNA replication past a bulky lesion catalyzed by the exo- Klenow fragment of pol I, *Biochemistry 40*, 6660−6669.
53. Jiang, G., Skorvaga, M., Van Houten, B., and States, J. C. (2003) Reduced sulfhydryls maintain specific incision of BPDE-DNA adducts by recombinant thermoresistant *Bacillus caldotenax* UvrABC endonuclease, *Protein Expression Purif. 31*, 88−98.
54. Van Houten, B., Gamper, H., Sancar, A., and Hearst, J. E. (1987) DNase I footprint of ABC excinuclease, *J. Biol. Chem. 262*, 13180−13187.
55. Huang, X., Colgate, K. C., Kolbanovskiy, A., Amin, S., and Geacintov, N. E. (2002) Conformational changes of a benzo[a]-pyrene diol epoxide-N(2)-dG adduct induced by a 5′-flanking 5-methyl-substituted cytosine in a (Me)CG double-stranded oligonucleotide sequence context, *Chem. Res. Toxicol. 15*, 438−444.
56. Moolenaar, G. F., Monaco, V., van der Marel, G. A., van Boom, J. H., Visse, R., and Goosen, N. (2000) The effect of the DNA flanking the lesion on formation of the UvrB-DNA preincision complex. Mechanism for the UvrA-mediated loading of UvrB onto a DNA damaged site, *J. Biol. Chem. 275*, 8038−8043.
57. Sancar, A. (1994) Mechanisms of DNA excision repair, *Science 266*, 1954−1956.
58. Buschta-Hedayat, N., Buterin, T., Hess, M. T., Missura, M., and Naegeli, H. (1999) Recognition of nonhybridizing base pairs during nucleotide excision repair of DNA, *Proc. Natl. Acad. Sci. U.S.A. 96*, 6090−6095.
59. Arghavani, M. B., SantaLucia, J., Jr., and Romano, L. J. (1998) Effect of mismatched complementary strands and 5′-change in sequence context on the thermodynamics and structure of benzo-[a]pyrene-modified oligonucleotides, *Biochemistry 37*, 8575−8583.
60. Breslauer, K. J., Frank, R., Blocker, H., and Marky, L. A. (1986) Predicting DNA duplex stability from the base sequence, *Proc. Natl. Acad. Sci. U.S.A. 83*, 3746−3750.
61. SantaLucia, J., Jr., Allawi, H. T., and Seneviratne, P. A. (1996) Improved nearest-neighbor parameters for predicting DNA duplex stability, *Biochemistry 35*, 3555−3562.
62. Chen, C., and Russu, I. M. (2004) Sequence-dependence of the energetics of opening of at basepairs in DNA, *Biophys. J. 87*, 2545−2551.
63. Fountain, M. A., and Krugh, T. R. (1995) Structural characterization of a (+)-trans-anti-benzo[a]pyrene-DNA adduct using NMR, restrained energy minimization, and molecular dynamics, *Biochemistry 34*, 3152−3161.
64. Xie, X. M., Geacintov, N. E., and Broyde, S. (1999) Stereochemical origin of opposite orientations in DNA adducts derived from enantiomeric anti-benzo[a]pyrene diol epoxides with different tumorigenic potentials, *Biochemistry 38*, 2956−2968.
65. Ruan, Q., Zhuang, P., Li, S., Perlow, R., Srinivasan, A. R., Lu, X. J., Broyde, S., Olson, W. K., and Geacintov, N. E. (2001) Base sequence effects in bending induced by bulky carcinogen-DNA adducts: experimental and computational analysis, *Biochemistry 40*, 10458−10472.
66. Protozanova, E., Yakovchuk, P., and Frank-Kamenetskii, M. D. (2004) Stacked-unstacked equilibrium at the nick site of DNA, *J. Mol. Biol. 342*, 775−785.
67. Ramstein, J., and Lavery, R. (1988) Energetic coupling between DNA bending and base pair opening, *Proc. Natl. Acad. Sci. U.S.A. 85*, 7231−7235.
68. Haase, I., Fischer, M., Bacher, A., and Schramek, N. (2003) Temperature-dependent presteady state kinetics of lumazine synthase from the hyperthermophilic eubacterium *Aquifex aeolicus*, *J. Biol. Chem. 278*, 37909−37915.
69. Kim, H. S., Damo, S. M., Lee, S. Y., Wemmer, D., and Klinman, J. P. (2005) Structure and hydride transfer mechanism of a moderate thermophilic dihydrofolate reductase from *Bacillus stearothermophilus* and comparison to its mesophilic and hyperthermophilic homologues, *Biochemistry 44*, 11428−11439.
70. Kohen, A., Cannio, R., Bartolucci, S., and Klinman, J. P. (1999) Enzyme dynamics and hydrogen tunnelling in a thermophilic alcohol dehydrogenase, *Nature 399*, 496−499.
71. Wang, Y. K., Morgan, A., Stieglitz, K., Stec, B., Thompson, B., Miller, S. J., and Roberts, M. F. (2006) The temperature dependence of the inositol monophosphatase Km correlates with accumulation of di-myo-inositol 1,1′-phosphate in *Archaeoglobus fulgidus*, *Biochemistry 45*, 3307−3314.
72. Bruice, T. C. (2006) Computational approaches: reaction trajectories, structures, and atomic motions. Enzyme reactions and proficiency, *Chem. Rev. 106*, 3119−3139.
73. Vieille, C., and Zeikus, G. J. (2001) Hyperthermophilic enzymes: sources, uses, and molecular mechanisms for thermostability, *Microbiol. Mol. Biol. Rev. 65*, 1−43.
74. Moolenaar, G. F., Hoglund, L., and Goosen, N. (2001) Clue to damage recognition by UvrB: residues in the beta-hairpin structure prevent binding to non-damaged DNA, *EMBO J. 20*, 6140−6149.
75. Machius, M., Henry, L., Palnitkar, M., and Deisenhofer, J. (1999) Crystal structure of the DNA nucleotide excision repair enzyme UvrB from *Thermus thermophilus*, *Proc. Natl. Acad. Sci. U.S.A. 96*, 11717−11722.
76. Nakagawa, N., Sugahara, M., Masui, R., Kato, R., Fukuyama, K., and Kuramitsu, S. (1999) Crystal structure of *Thermus thermophilus* HB8 UvrB protein, a key enzyme of nucleotide excision repair, *J. Biochem. (Tokyo) 126*, 986−990.
77. Yang, W. (2006) Poor base stacking at DNA lesions may initiate recognition by many repair proteins, *DNA Repair 5*, 654−666.
78. Patel, D. J., Pardi, A., and Itakura, K. (1982) DNA conformations, dynamics, and interactions in solution, *Science 216*, 581−590.
79. Malta, E., Moolenaar, G. F., and Goosen, N. (2006) Base flipping in nucleotide excision repair, *J. Biol. Chem. 281*, 2184−2194.

BI700294K